The Astrophysical Journal, 871:15 (10pp), 2019 January 20 https://doi.org/10.3847/1538-4357/aaf6b2

Infrared Echo and Late-stage Rebrightening of Nuclear Transient Ps1-10adi: Exploring the Torus with Tidal Disruption Events in Active Galactic Nuclei

Ning Jiang[1,2], Tinggui Wang[1,2], Guobin Mou[3], Hui Liu[1,2], Liming Dou[4], Zhenfeng Sheng[1,2], and Yibo Wang[1,2]
[1] Key Laboratory for Research in Galaxies and Cosmology, Department of Astronomy, University of Science and Technology of China, Chinese Academy of Sciences, Hefei, Anhui 230026, People's Republic of China; jnac@ustc.edu.cn
[2] School of Astronomy and Space Sciences, University of Science and Technology of China, Hefei, Anhui 230026, People's Republic of China
[3] School of Physics and Technology, Wuhan University, Wuhan 430072, People's Republic of China
[4] Center for Astrophysics, Guangzhou University, Guangzhou 510006, People's Republic of China
Received 2018 August 10; revised 2018 November 27; accepted 2018 December 4; published 2019 January 18

Abstract

Tidal disruption events (TDEs) in active galactic nuclei (AGNs) have been overlooked for a long time but have recently been tentatively investigated. We report the discovery of a long-lasting, luminous mid-infrared (mid-IR) flare in PS1-10adi, which is a newly identified and highly energetic transient event occurring in an AGN. The IR luminosity of PS1-10adi, as well as other analogous events, is at least one order of magnitude higher than that of all known supernova, but can be well interpreted as the dust echoes of TDEs, whose ultrahigh IR energy is reprocessed from the dusty torus around the black hole. The torus dust is sublimating during the early stage of the outburst and probably leads to the observed rapid emergence of Fe II lines. Moreover, the UV-optical rebrightening and contemporaneous X-ray onset after ∼1500 rest-frame days since the optical peak are also an intriguing feature of PS1-10adi that can be attributed to the interaction between the high-velocity outflow and the torus. We suggest that the luminous IR echo is a very typical phenomenon of TDEs in AGNs and may provide us an ideal opportunity to explore the torus properties.

Key words: galaxies: active – galaxies: individual (PS1-10adi) – galaxies: nuclei – infrared: galaxies

1. Introduction

The stellar or gas kinematics on nearby galaxies in the past two decades have established that supermassive black holes (SMBHs), with masses of $10^{6-10}\,M_{\odot}$, are universal in the centers of galaxies with massive bulges. Furthermore, the tight correlations between the BH mass ($M_{\rm BH}$) and various bulge properties indicate an attractive coevolutionary growth of SMBHs and their host galaxies (see reviews by Kormendy & Ho 2013 and Heckman & Best 2014). The widespread picture is not unquestionable; there are some alternative views, which claim that their relation can emerge as the result of a statistical convergence process without a physical coupling (e.g., Peng 2007; Jahnke & Macciò 2011), or the dark matter might be influential (e.g., Ostriker 2000; Zhao et al. 2002; Bogdán & Goulding 2015). In any case, SMBHs are normally believed to accumulate their mass through the phase of active galactic nuclei (AGNs), during which the BHs are efficiently accreting surrounding materials. AGNs themselves are also the best evidence of the existence of SMBHs in distant galaxies, which are otherwise beyond the current capabilities for direct dynamical measurement.

Nevertheless, the detection of SMBHs in normal galaxies is still very difficult given that the vast majority of them are quiescent and far away. Although some new approaches seem promising for detecting SMBHs at cosmological distances, such as gravitational lensing (e.g., Mao et al. 2001; Hezaveh et al. 2015; Chen et al. 2018) and future gravitational wave observations of SMBH mergers or the inspiral of compact stellar remnants consumed by SMBHs, they are not efficient and practical for the time being. In one opportunity, the so-called tidal disruption event (TDE) could offer us the greatest chance to catch sight of these dormant SMBHs. The TDE happens if a star in the galaxy wanders too close to the central black hole: the star can be ripped apart when the tidal force exceeds its self-gravity, and roughly half the mass of the star will be accreted onto the black hole while the remaining half may be ejected, by the simple classical theory (Rees 1988). Recent works reveal that the real accreting fraction could be much lower because most of the mass may join an outflow (e.g., Metzger & Stone 2016). A luminous flare of electromagnetic radiation is expected during this process, with emission peaks in the UV or soft X-rays and a characteristic $t^{-5/3}$ decline on a timescale of months to years (Rees 1988; Phinney 1989). The TDE event rate is estimated to be 10^{-4} to 10^{-5} galaxy^{-1} yr^{-1} and might be at its highest in nucleated dwarf galaxies (Wang & Merritt 2004; Stone & Metzger 2016).

Observationally, though TDEs were first discovered in X-ray bands serendipitously, the field did not experience explosive growth until the past decade, benefiting from a batch of dedicated optical time-domain surveys (see Komossa 2015 as a review). To avoid any potential contaminations stemming from variability of AGNs, traditional searches of TDEs have solely cared about normal galaxies and neglected active galaxies (e.g., van Velzen et al. 2011). However, TDEs might also occur in AGNs, and the rates are even expected to be high (Karas & Šubr 2007), not to mention that TDEs were actually first proposed as a possible power source of AGNs and quasars (Hills 1975). Recently, Blanchard et al. (2017) claimed a TDE candidate PS16dtm found in the Panoramic Survey Telescope and Rapid Response System (Pan-STARRS). This event occurs in a Seyfert 1 galaxy with $M_{\rm BH} \sim 10^6\,M_{\odot}$ and displays some distinctive features, such as a plateau phase, disappeared prior X-ray emission, and newly emerging strong Fe II emission. Soon thereafter, Kankare et al. (2017, hereafter K17) reported another highly energetic Pan-STARRS transient event named PS1-10adi that had a total radiated energy of $\sim 2.3 \times 10^{52}$ erg. The rapid, smooth brightening light curve and persistently narrow spectral lines over ∼3 yr from PS1-10adi are

inconsistent with known types of recurring BH variability, yet may be linked to a TDE or supernova (SN) in the nuclear region powered by shock interaction between expanding material and large quantities of surrounding dense matter. K17 have even unveiled the possibility of a population of such events existing in the centers of active galaxies yet to be further explored.

Encouraged by our successful detection of a mid-infrared (mid-IR) flare in PS16dtm and valuable implications learned from it (Jiang et al. 2017), we have also checked the mid-IR variability of PS1-10adi and discovered a long-lasting flare not surprisingly in a location coincident with PS1-10adi using data from the *Wide-field Infrared Survey Explorer* (*WISE*; Wright et al. 2010; Mainzer et al. 2014). In addition, we have noticed an odd late-stage rebrightening in the UV-optical light curve as well as a corresponding mid-IR signal. The mid-IR emission in radio-quiet AGNs is generally thought to be associated with thermal emission from dust at parsec-scale distances from the central SMBH. On the other hand, an optically thick obscuring medium in the equatorial plane (commonly dubbed the "torus") is needed in the unified model; the current paradigm suggests that the IR-emitting dust is the same medium as the obscuring material. This is reflected in the widespread use of torus models in order to reproduce IR spectral energy distributions (SEDs; see a recent review on torus models in Netzer 2015). Based on the fact of a preexisting dusty torus, mid-IR echoes are predictable for those TDEs in active galaxies, which would expose the torus itself dynamically. The ubiquitous luminous IR echoes associated with TDEs in AGNs may be one of the most notable characteristics distinguishing them from SNe (see Section 5).

In this paper, we will try to analyze all of these newly recognized phenomena in PS1-10adi and understand them in the context of TDEs in AGNs. We assume a cosmology with $H_0 = 70$ km s^{-1} Mpc^{-1}, $\Omega_m = 0.3$, and $\Omega_\Lambda = 0.7$. At a redshift of $z = 0.203$, PS1-10adi has a luminosity distance of 996.5 Mpc.

2. Mid-IR Light Curves

The *WISE* has performed a full-sky imaging survey in four broad mid-IR bandpass filters centered at 3.4, 4.6, 12, and 22 μm (labeled *W*1–*W*4) from 2010 February to August. The solid hydrogen cryogen used to cool the *W*3 and *W*4 instrumentation was later depleted, and it was placed in hibernation in 2011 February. *WISE* was reactivated and renamed NEOWISE-R in 2013 October, using only *W*1 and *W*2, to hunt for asteroids that could be an impact hazard to Earth. *WISE* has scanned a specific sky area every half year and thus yielded 10–11 observations for every object up to now. For each epoch, there are 10–20 single exposures. We use only the best-quality single-frame images by selecting only detections with data quality flag "qual_frame" > 0.

PS1-10adi is a point-like source in *WISE* images without any potential contamination within 10″. We have collected all of its public *WISE* photometric data, including from the ALLWISE and NEOWISE-R catalogs. The data are distributed in 10 epochs at intervals of about six months from 2010 May 9 (MJD = 55,325) to 2017 October 22 (MJD = 58,048). The light curves in *W*1 and *W*2 are presented in Figure 1. For ease of comparison, its optical light curve (*V*-band) has also been overplotted. First, no reliable variability is detected within each epoch, so we average these data to obtain a mean value at each

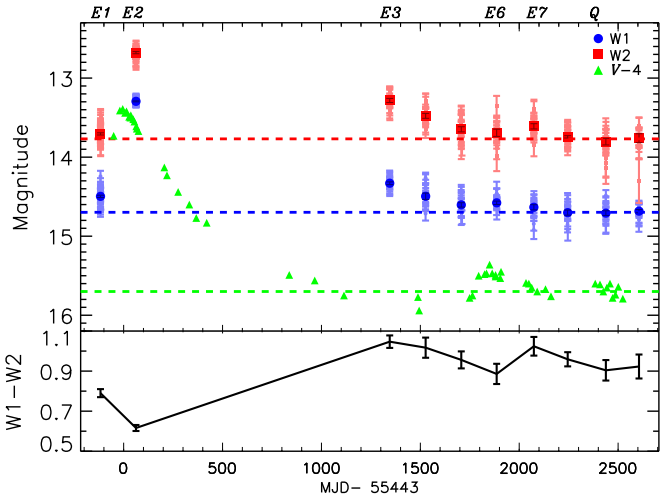

Figure 1. *WISE W*1 (3.4 μm, blue squares) and *W*2 (4.6 μm, red triangles) light curves of PS1-10adi. The horizontal dashed lines represent the background magnitudes estimated from the latest three epochs. The *V*-band light curve is also plotted for comparison (green triangles). The *W*1–*W*2 color is shown in the bottom panel.

epoch, as in our previous works (Jiang et al. 2012, 2016). We noticed that the first *WISE* epoch ("E1") is 98 days before and the second epoch ("E2") is 82 days after the optical discovery date, or −117 (rest-frame − 97) days and 63 (52) days since the optical peak. PS1-10adi began brightening by ∼1 mag in *W*1 and *W*2 at E2 relative to E1. Unfortunately, *WISE* went into hibernation soon after and did not yield the third observation until 2014 May, resulting in a gap of 1282 days between E2 and E3. The light curve presents a declining trend at E3 and thereafter and remains at a constant level in the recent past. In order to isolate the host galaxy and AGN emission (or background emission as a whole) from the outburst phase, we take the last three epochs as the quiescent state, which contributes an averaged magnitude of 14.70 ± 0.02 and 13.77 ± 0.03 at *W*1 and *W*2, respectively. The original and background-subtracted magnitudes are shown in Table 1. It is interesting to note that PS1-10adi is already brighter at E1, by 0.20 ± 0.02 and 0.06 ± 0.03 magnitudes in *W*1 and *W*2, respectively. The *W*1–*W*2 color has generally been used as a rough assessment of the AGN or stellar dominance of a galaxy; for instance, *W*1–*W*2 > 0.8 for AGN-like or *W*1–*W*2 < 0.5 for galaxy-like (Stern et al. 2012; Yan et al. 2013). The *W*1–*W*2 at E1 is 0.79 ± 0.02, significantly lower than 0.93 ± 0.05 at the last three epochs (see bottom panel of Figure 1), likely indicating that it is experiencing an extra-high energy input in addition to the AGN at E1. Therefore, we think that the flux excess at E1 is not simply due to AGN variability.

K17 presented UV-optical-IR light curves of PS1-10adi up to ∼2200 days since the peak (see their Supplementary Figure 1). When we look through them carefully, we note that there is a tiny yet notable hump at MJD ≈ 57,293 (identified as the "2015 bump" in K17). For ease of convenience, we call the first major flare the "primary outburst" and the second peak "rebrightening." Interestingly, the rebrightening also occurs subsequently in *W*1 and *W*2, in which the *W*2 lags behind *W*1 by about one-half year. The *W*1 and *W*2 magnitudes have brightened by 0.12 ± 0.03 (4σ) and 0.08 ± 0.05 (1.6σ) at E6, and by 0.06 ± 0.04 (1.5σ) and 0.16 ± 0.04 (4σ) at E7, respectively.

Table 1
WISE Data

Epoch (1)	MJD (2)	W1m (3)	W2m (4)	*W1* (5)	*W2* (6)	*W1*–*W2* (7)	log L_{W1} (8)	log L_{W2} (9)	T_{dust} (10)	log L_{dust} (11)
E1	55325	14.50 ± 0.01	13.71 ± 0.01	16.42 ± 0.02	16.83 ± 0.03	−0.41	42.9	42.4	…	…
E2	55505	13.29 ± 0.01	12.68 ± 0.01	13.64 ± 0.01	13.17 ± 0.03	0.47	44.1	43.9	1972	44.3
E3	56788	14.33 ± 0.02	13.28 ± 0.03	15.68 ± 0.02	14.39 ± 0.04	1.29	43.2	43.3	886	43.5
E4	56969	14.50 ± 0.04	13.48 ± 0.03	16.42 ± 0.04	15.50 ± 0.04	1.37	42.9	43.1	843	43.2
E5	57150	14.60 ± 0.03	13.65 ± 0.03	17.31 ± 0.03	16.09 ± 0.05	1.22	42.6	42.7	927	42.8
E6	57329	14.58 ± 0.02	13.69 ± 0.05	17.03 ± 0.03	16.60 ± 0.06	0.43	42.7	42.5	2114	43.0
E7	57517	14.63 ± 0.03	13.61 ± 0.03	17.75 ± 0.04	15.77 ± 0.05	1.98	42.4	42.8	620	43.1
Q	57881	14.70 ± 0.02	13.77 ± 0.03	…	…	0.93	…	…	…	…

Note. Column (1): observational epochs. Column (2): median modified Julian date. Columns (3)–(4): median *W1* and *W2* magnitudes. Columns (5)–(6): background-subtracted *W1* and *W2* magnitudes. Column (7): background-subtracted *W1*–*W2* color. Columns (8)–(9): background-subtracted *W1* and *W2* monochromatic luminosity. Column (10): dust temperature inferred from *W1*–*W2* color assuming blackbody radiation. Column (11): the logarithmic integrated dust blackbody luminosity.

3. Evaporation and Echo of Torus Dust

3.1. Infrared Echo of Torus Dust

The IR flares detected in TDEs thus far are all successfully translated into dust echoes (Dou et al. 2016, 2017; Jiang et al. 2016, 2017; van Velzen et al. 2016). The dust, if there, in the vicinity of SMBHs will certainly absorb the primary emission of TDEs (soft X-ray, UV, and optical) and reprocess it into IR, so we expect the flare in the IR would lag behind the optical (Lu et al. 2016). However, in some cases, the mid-IR variability could be detectable even earlier than the optical band, and thus the echo interpretation is not so obvious. For example, we recently found a mid-IR flare that started ∼11 days before the optical detection of TDE candidate PS16dtm (Jiang et al. 2016). Interpreting the mid-IR flare as a dust echo requires close preexisting dust with a high covering factor, which is fully qualified with the geometrically and optically thick torus in AGNs. The case in PS1-10adi looks even more extreme, in which the mid-IR brightening is detectable 118 (or rest-frame 98) days earlier than the optical discovery. Can it be explained by the scenario of PS16dtm as well?

The AGN property before the outburst is unfortunately missing because of a lack of observations, yet can be supposed to be almost the same as the postflare state. For the sake of an estimate, we have fitted the optical spectra at +1600 days (see Supplementary Figure 2 of K17) and obtained that the broad Hα luminosity ($L_{H\alpha}$) is 8.8×10^{41} erg s^{-1} with an FWHM of 3676 km s^{-1}. By virtue of the empirical relation of M_{BH} in AGNs estimated from the luminosity and FWHM of the broad Hα line (Greene & Ho 2005), the M_{BH} is 2.7×10^7 M_{BH}. Using the bolometric correction given by Greene & Ho (2007), the bolometric luminosity (L_{bol}) is $2.34 \times 10^{44}(L_{H\alpha}/10^{42})^{0.86} = 2.1 \times 10^{44}$ erg s^{-1}. The peak background-subtracted L_{bol} associated with the flare inferred from the UV-optical emission is $\sim 5 \times 10^{44}$ erg s^{-1} (see Figure 2), so the total peak L_{bol} is $\sim 7 \times 10^{44}$ erg s^{-1}, provided that all of the radiation originates from the BH accretion.

In order to assess if the energy budget for the dust echo is reasonable, we have fitted the background-subtracted UV-optical-IR SEDs at different epochs using a double-blackbody model, one for the original outburst emission dominating the UV-optical band, and the other for the reprocessed dust emission peaked in the IR (see an example in the top panel of Figure 3). We take the integrated luminosity of the blue component as the L_{bol} (see its evolution in Figure 2). Since

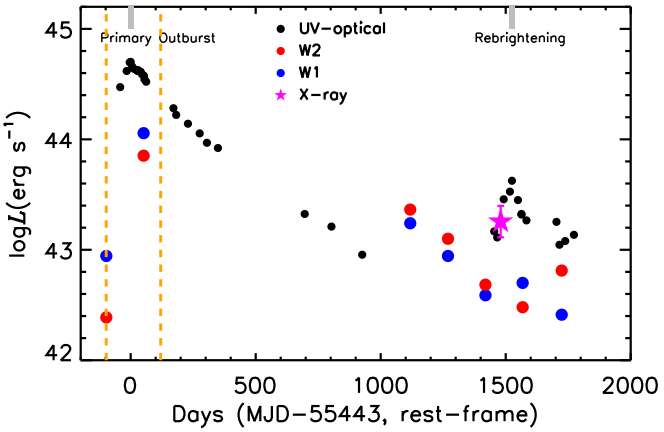

Figure 2. Luminosity evolution of PS1-10adi. The black, blue, and red dots represent the UV-optical blackbody fitted luminosity and *WISE* *W1* and *W2* luminosity, respectively. We have marked the peak time of the primary outburst and the rebrightening. The X-rays detected during the rebrightening are plotted as a magenta five-pointed star. The region between the two orange dashed lines denotes the time when the torus dust is sublimating.

there is no reliable detection of residual UV-optical emission at E1, a single blackbody is adopted and yields an ultrahigh dust temperature of $\sim 10^7$ K. This value seems absolutely unreasonable and is probably due to a nonequilibrium condition, a too-simplified model, and the insensitivity to the slope of the Rayleigh–Jeans tail for a very high blackbody temperature. Therefore, we believe that the dust at E1 is sublimating in spite of the very uncertain dust temperature.

The double-blackbody fitting at E2 yields a dust temperature (T_{dust}) of 2150 ± 430 K, which is consistent with the dust sublimation temperature within error (see also K17). Assuming that the equilibrium T_{dust} of a dust grain with radius a at distance R from the heating source is determined by the balance between the radiative heating by UV-optical photons and the thermal reemission in the IR, we have

$$\frac{L_{bol}}{4\pi R^2}\pi a^2 = 4\pi a^2 \sigma T^4. \quad (1)$$

The calculated L_{bol} is 1.1×10^{45} erg s^{-1} given a dust distance $R = 52$ light days by the time lag to the optical peak. The value is slightly higher yet comparable to the observed peak L_{bol}

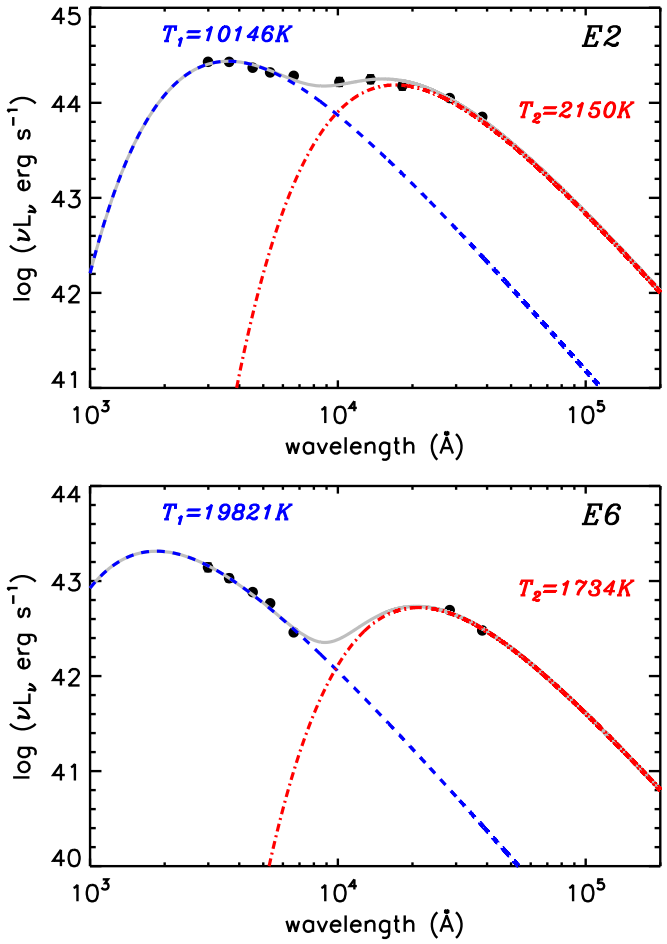

Figure 3. Background-subtracted SED of PS1-10adi at E2 (MJD ≈ 55,505) and E6 (MJD ≈ 57,323). The optical-NIR photometry is drawn from supplementary Tables 2 and 3 of K17. We have tried to fit the SED using a double-blackbody model, one for the UV-optical emission (blue dashed line) and the other for the dust emission (dot-dashed line).

($L_{\rm peak}$) of 7×10^{44} erg s^{-1}, providing valid evidence for the dust echo interpretation.

3.2. Evaporation of Torus Dust and Fe II Emergence

The torus inner radius can be computed by the dust sublimation radius ($R_{\rm sub}$) below (here we used the formula given in Namekata & Umemura 2016):

$$R_{\rm sub} = 0.121\ {\rm pc}\left(\frac{L_{\rm bol}}{10^{45}\ {\rm erg\ s^{-1}}}\right)^{0.5}\left(\frac{T_{\rm sub}}{1800\ {\rm K}}\right)^{-2.804} \times \left(\frac{a}{0.1\ \mu{\rm m}}\right)^{-0.510}. \quad (2)$$

The original torus inner radius is determined by the $L_{\rm bol}$ before the primary outburst, whose corresponding $R_{\rm sub}$ is 5.6×10^{-2} pc, that is, 66 light days. As the luminosity of PS1-10adi increases, the illuminated dust in the inner region evaporates gradually, pushing the inner side of the dusty torus outward. The calculation at the optical peak yields a new $R_{\rm sub}$ of 0.10 pc (∼120 light days), so the preexisting dust located between 66 and 120 light days should have been evaporated.

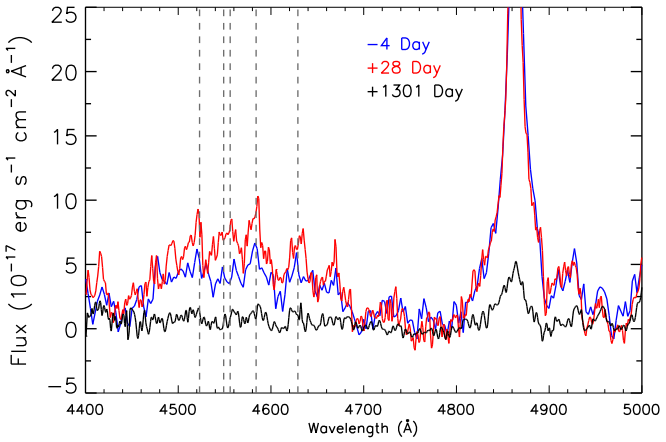

Figure 4. Variability of optical Fe II emission of PS1-10adi (data drawn from K17). Three spectra taken at −4 (blue), +28 (red), and +1301 days (black) with respect to the optical peak are presented after the subtraction of the continuum. The positions of the Fe II lines are marked as dashed gray lines. The Fe II intensity strengthened at the early stage (from −4 to 28 days) but had faded by the end of the event (+1301 days).

The dust sublimation as a function of temperature can be estimated by

$$\frac{dm}{dt} = -\rho\, A\, \nu_0 \left(\frac{\mu}{\rho}\right)^{1/3} e^{-B/kT}. \quad (3)$$

We adopt $\rho = 2.5$ g cm^{-3}, $\nu_0 \simeq 10^{15}$ s^{-1}, $B/k = 7 \times 10^4$ K, and $\rho/\mu = 10^{23}$ cm^{-3} following Equation (7) of Lu et al. (2016); these are representative values for refractory grains (Guhathakurta & Draine 1989; Waxman & Draine 2000). Here, A is the total illuminated dust area, which is 1.7×10^{35} cm^2 at E2 ($A = L_{\rm dust}/\sigma T^4$), giving a dust sublimation rate $dm/dt = 1.0 \times 10^{26}$ g s^{-1}. The precise mass of evaporated dust is difficult to determine because of the poor sampling of the light curves. We hypothesize that the sublimation rate at E2 is an average value between −98 and +120 days (region between the two orange dashed lines in Figure 2); the integrated evaporated dust is thus $\sim 1.9 \times 10^{33}$ g, that is, around 1 $M_\odot$.

Similar to the story told in PS16dtm (Jiang et al. 2017), metals originally reserved in the evaporated dust will enter the gas and may be ionized, giving rise to metal lines, such as the Fe II multiplets observed in PS1-10adi (Figure 4; see also Supplementary Figure 2 in K17), making it resemble a classical narrow-line Seyfert 1 galaxy. If we believe that metals are mostly locked in the dust and the gas holds the solar metallicity, the gas mass should be higher than the dust mass by a factor of $\alpha \sim 50$. Supposing that the gas is distributed in the spherical region (outer radius $R_{\rm o} = 120$ light days) with a covering factor of $f_{\rm c}$, the column density of the new broad-line region (BLR) can be calculated as below:

$$N_{\rm H} = \frac{\alpha\, m_{\rm dust}}{4\pi\, f_{\rm c}\, R_{\rm o}^2\, m_{\rm H}}. \quad (4)$$

The derived $N_{\rm H}$ is 1.2×10^{23} cm^{-2}, in which we have adopted $f_{\rm c} = 0.4$ (see Section 5.3). Both the gas mass and $N_{\rm H}$ of the new BLR here are comparable to that of typical AGNs (Peterson 1997; Netzer 2013), indicating that they are likely sufficient to produce the observed Fe II strength even if the physical mechanisms are still not yet very clear. Note that the Fe II multiplets have almost vanished after the outburst (see its

+1301 day spectrum in Figure 4), agreeing well with the photoionization model.

Many previous studies show that the photoionization cannot fully address the Fe II emission of AGNs (Collin & Joly 2000; Sigut & Pradhan 2003; Baldwin et al. 2004); collisional excitation might also act (e.g., Joly 1981; Véron-Cetty et al. 2006). This could be feasible in TDEs because the unbound debris ejected from the disrupted star may cause shocks by interacting with the gas and excite the iron. One needs to illustrate whether the time of collision is early enough to result in the instant presence of Fe II. The maximum escaping velocity of the unbound debris $v_{\rm max} = (2GM_{\rm BH}R_*/R_t^2)^{1/2} = 9 \times 10^3$ km s^{-1} in the case of one solar-mass star disrupted by a $\sim 10^7 M_\odot$ BH, so the timescale of reaching the torus is $r_{\rm torus}/v_{\rm max} = 6$ yr given an $r_{\rm torus}$ of 66 light days. For the bound debris, although the circularization process is still not yet fully understood, several simulations show that the circularization timescale is in the range of several times to $\sim$10 times the orbital period of the most bound debris (Bonnerot et al. 2016; Hayasaki et al. 2016). The period of the most bound debris can be estimated by $T_{\rm min} = 2\pi GM_{\rm BH}\,(-2\epsilon_{\rm min})^{-3/2}$, in which $\epsilon_{\rm min} = -GM_{\rm BH}\,R_*/R_t^2$ is the lowest specific mechanical energy. The derived $T_{\rm min} \sim 0.6$ yr, meaning that the circularization timescale could also be as long as years yet with large uncertainties.

In brief, we surmise that the rapid emergence of prominent Fe II lines could be a universal characteristic of TDEs in AGNs, which will potentially allow us to understand the origin of Fe II emission in AGNs.

4. Late-stage Rebrightening

4.1. Late Accretion?

The rebrightening hump that appeared in the UV-optical light curve is nonnegligible, but it was not discussed in K17. As it happens, a similar hump is also present in the mid-IR light curve, with the $W1$ band ahead of $W2$. Besides that, the X-ray emission was first detected with a 0.3–10 keV luminosity of 2×10^{43} erg s^{-1} during the rebrightening (see Supplementary Table 4 of K17). Unfortunately, the photons are too few to constrain whether it is dominated by soft X-rays or not.

First, we attempt to naively understand the rebrightening as a late-stage accretion. The peak $L_{\rm bol}$ of the rebrightening is lower than the primary outburst by one order of magnitude; the time delay of dust emission relative to the rebrightening should be $\sim$100 days as long as no dust newly formed. The fitted $T_{\rm dust}$ at E6 is 1.7×10^3 K, and then it drops quickly to $\sim 6 \times 10^2$ K at E7. The mid-IR emission at E6 requires $L_{\rm bol} \approx 1.7 \times 10^{45}$ erg s^{-1} according to Equation (1), which is two orders of magnitude higher than the observed $L_{\rm bol}$ at $\sim$100 days before E6. One way to resolve the conflict is to remember that the blackbody assumption for dust emission could be oversimplistic and the dust absorption efficiency ($Q_{\rm abs} \propto \nu^\beta$) should be taken into account. The β value is quite uncertain: it approaches zero for very large grains (gray case), while for small grains, β strongly depends on the composition, at $\simeq$2 for graphite, $\simeq$1 for silicate, and $\simeq -0.5$ for SiC. If we adopt $\beta = 2$ (see formula 8.16 in Kruegel 2003),

$$\frac{L_{\rm bol}}{16\pi^2 R^2} \simeq 1.47 \times 10^{-6} a T^6, \quad (5)$$

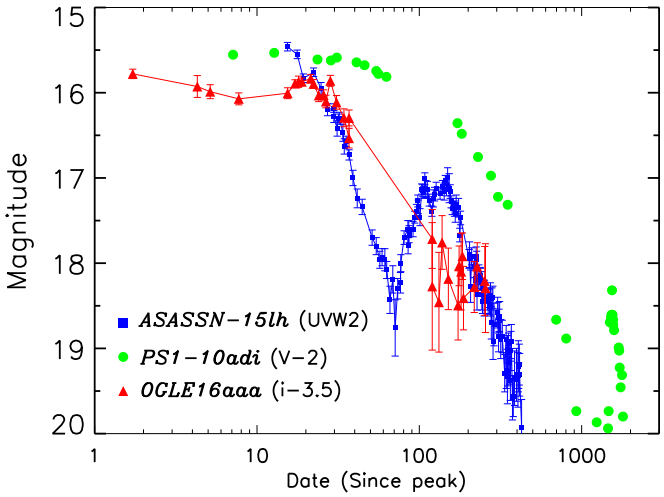

Figure 5. Comparison of the three TDE candidates with rebrightening-like light curves. Apart from the late-stage rebrightening of PS1-10adi (green dots), ASASSN-15lh presents a giant double-peaked light curve (blue squares, data from Godoy-Rivera et al. 2017), yet OGLE16aaa (red triangles, data from OGLE-IV Transient Detection System (http://ogle.astrouw.edu.pl/ogle4/transients/2017a/transients.html) shows a slight rebrightening at an earlier stage.

we get $T_{\rm dust} = 1.0 \times 10^3$ K, calling for an $L_{\rm bol}$ of 1.3×10^{43} erg s^{-1} for dust with an MRN (Mathis–Rumpl–Nordsieck) size distribution (Mathis et al. 1977), which is still comparable with the observation. However, it is hard to imagine that the dust properties responsible for E2 and E6 are so different. The other negative evidence stems from the concomitant X-ray emission, which is strangely absent in the early accretion but not in the late accretion. Therefore, we conclude that the late-stage accretion scheme is very unlikely.

4.2. Rebrightening in Other TDEs

We have noticed that among the reported TDEs, ASASSN-15lh and OGLE16aaa also show a rebrightening characteristic in their UV-optical light curves (see Figure 5). In fact, it is exactly the giant double-humped feature that motivated reconsideration of the nature of ASASSN-15lh, which was first claimed to be an unprecedentedly luminous SNe in view of its spectral resemblance to a hydrogen-poor superluminous SN (SLSN) at an early stage (Dong et al. 2016). Together with several other lines of evidence from further monitoring (e.g., temperature evolution), ASASSN-15lh can be also understood as a TDE occurring in a spinning BH with mass of $3 \times 10^8\,M_\odot$ (Leloudas et al. 2016; Krühler et al. 2018) rather than a supernova. Coincidentally, the X-ray emission was not detected in ASASSN-15lh either until the rebrightening, which was about 4 months after the primary peak (Margutti et al. 2017). Both circularization (Guillochon & Ramirez-Ruiz 2015) and reprocessing (Metzger & Stone 2016) models have been suggested as possible ways to address the intriguing UV-optical light curve (Leloudas et al. 2016). The rebrightening of OGLE16aaa is visible, yet much less obvious than in ASASSN-15lh. Wyrzykowski et al. (2017) tried to explain the variability as being induced by a binary BH on a tight orbit or being due to disk precession or circularization on a timescale of about a month. *Swift* observations taken around the same time of the optical flare detected no X-ray emission. However, further *Swift* exposures at $\sim$140 dates later enabled us to detect

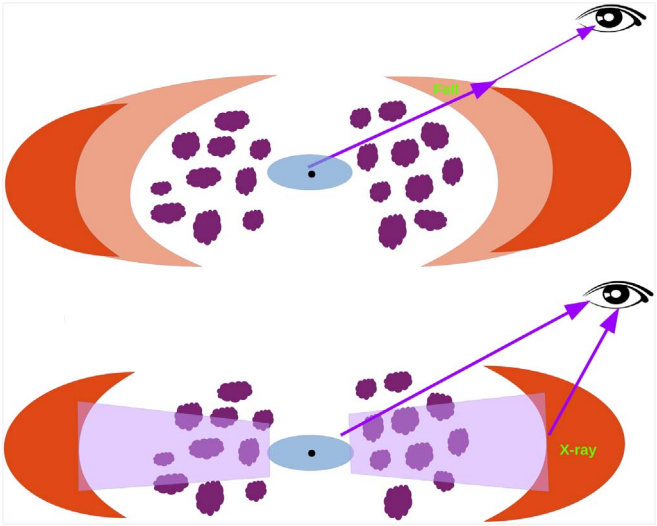

Figure 6. Schematic of the PS1-10adi model. In the standard AGN unification, the SMBH (black solid circle), accretion disk (blue ellipse), BLR (aubergine clouds), and torus (orange tori) are distributed from inside to outside. Top panel: the central engine of PS1-10adi was partly obscured by the torus yet largely exposed after the TDE after the receding of the torus. The metals released from the evaporated dust (light orange region) will give rise to the observed strong Fe II lines. Bottom panel: the high-speed outflow (denoted as light purple) launched from the accretion disk collides with the torus and produces the late-stage rebrightening and X-ray onset.

significant X-ray emission from this event, which then decayed and faded over a few months (Auchettl et al. 2017).

Both the rebrightening and the associated X-ray onset in ASASSN-15lh and OGLE16aaa are similar to that in PS1-10adi, indicating plausibly a common and unified phenomenon in TDEs waiting to be understood. However, PS1-10adi is still somehow different from the other two. First, the time of the rebrightening relative to the primary outburst is much later (see Figure 5), at some 1500 days, when the TDE emission has almost disappeared. Second, the parsec-scale gas and dust around the SMBH of PS1-10adi should be pretty ample, evidenced by the intense usual AGN activity and high dust covering factor revealed by the dust echo (see Section 5). In contrast, the nuclei of ASASSN-15lh and OGLE16aaa are relatively quiescent despite weak AGN signatures (Wyrzykowski et al. 2017; Krühler et al. 2018).

4.3. Interaction between Debris or Outflow and the Torus

The particularities of PS1-10adi encouraged us to come up with possible new mechanisms of the rebrightening. Could it be caused by the collision between the unbound stellar debris and the interstellar medium (ISM) at the scale of an AGN torus? The spread of specific orbital energy $\Delta\epsilon = GM_{\rm BH}R_*/R_t^2$ is almost a constant for a large range of $\beta \equiv r_t/r_p$ (Stone et al. 2013; Tejeda et al. 2017). The total orbital energy of unbound debris is $\Delta E < 0.5M_\odot \times 0.5\Delta\epsilon$. The interaction timescale for this collision is $t_{\rm intact} \sim 0.5r_{\rm torus}/0.5v_{\rm max} = r_{\rm torus}/v_{\rm max} \sim$ 1500 days. Therefore we can estimate the upper limit of rebrightening power assuming that all of the orbital energy can be transferred into the gas internal energy and radiate efficiently: $L_X({\rm max}) < \Delta E/t_{\rm intact} = 1.5 \times 10^{42}$ ergs s^{-1}, which is one order of magnitude lower than observations. As a result, we argue that the rebrightening may not be due to the collision between the unbound debris and the torus.

Apart from the ejected debris, outflows launched by the TDE can also serve as a source of collision (see Figure 6 as an illustration). If that is the case, the observed outflow velocity can be estimated by $v_{\rm ej} = r_{\rm torus}/t_{\rm reb} \sim 120/1500 * c = 2.4 \times 10^4$ km s^{-1}. Outflows with such a high velocity have been found in observations (e.g., Blanchard et al. 2017; Kara et al. 2018) and numerical simulations in which the outflow may be produced during the self-crossing process under the general relativistic precessing (e.g., Jiang et al. 2016; Sądowski et al. 2016), or from the final accretion disk with a super-Eddington accretion rate (e.g., Dai et al. 2018). For example, in the simulation of Sądowski et al. (2016), about 10% of the star's total mass can be transferred into the outflow after the violent self-crossing, with an outflowing velocity of $\sim$0.1 c (yet we should stress that the object simulated therein is a 0.1-solar-mass star tidally disrupted by a BH of $10^5\,M_\odot$). Hence the total kinetic energy of this outflow is on the order of 10^{50} ergs. As a comparison, the integrated UV-optical bolometric light curve between 1500 and 2000 rest-frame days results in a total energy of $\sim 5 \times 10^{50}$ erg, which is on the same order of magnitude as the self-crossing outflow. In the interacting torus model, both the primary collisional and dust-reprocessed emission are almost local, which can naturally address the high $T_{\rm dust}$ at the rebrightening stage. This is also supported by the time lag between the optical and IR rebrightening, which is shorter than the light travel time from the BH to the new torus boundary ($\sim$100 days).

Last, we caution that besides the torus dust distributed in the equatorial plane around the accretion disk, dust elongated in the polar direction has also been found in both type 1 and type 2 AGNs via recent mid-IR interferometry observations (Hönig et al. 2013) and SED fitting (Lyu & Rieke 2018; Mattila et al. 2018). It is suggested that a radiatively driven dusty wind, possibly launched in a puffed-up region of the inner hot part of the torus, is responsible for the polar dust (Hönig et al. 2012). The dusty wind is mostly optically thin and extends in the polar direction over parsecs or even tens of parsecs. On the other hand, the polar outflow is not inhibited inherently and has been tentatively reported in some broad absorption line quasars (e.g., Zhou et al. 2006). Therefore, the collision between the polar outflow and the polar dust cannot be excluded completely in producing the observed rebrightening.

5. Revisiting the Nature of PS1-10adi and Analogs

In previous sections, we have assumed that the nuclear transient in PS1-10adi is a TDE and have tried to understand all observations in the context of TDEs. However, as mentioned in K17, the case of an extraordinary bright SNe occasionally exploding in the galactic nucleus is still impossible to disentangle from the TDE case up until then. In this section, we will try to revisit the nature of PS1-10adi and other similar events with the aid of mid-IR light curves.

5.1. Mid-IR Light Curves of PS1-10adi Analogs

Besides PS1-10adi, K17 reported five other outbursts in the centers of active galaxies. They constitute the sample of highly energetic nuclear transient events along with PS1-10adi. To understand their nature as a whole, we have retrieved their *WISE* and NEOWISE photometric data and presented the light curves in Figure 7. Significant mid-IR flare-like variability is visible for them all. As we already know the optical peak date

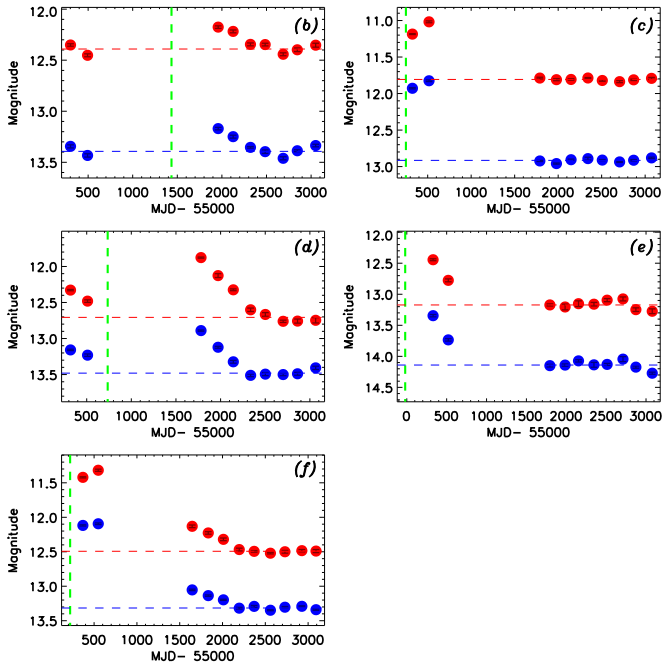

Figure 7. *WISE W*1 (blue) and *W*2 (red) light curves of PS1-10adi analogs reported in K17. (b–f) PS1-13jw, CSS100217, J094608, J094806, and J233454. The green dashed line marks the optical peak date.

of these events, we first estimated the background emission unassociated with the outbursts by averaging the magnitudes before or after the flares when the light curves are maintained a stable level.

It is interesting to note that a sustained mid-IR excess is present in J094608 before the optical flare. To exclude the probability of a spurious signal caused by a systematic bias between ALLWISE and NEOWISE-R data, we have performed aperture photometry on the time-resolved coadds of *WISE* images (Meisner et al. 2018). The excess ahead of the optical flare is proven to be real. It may be simply attributed to a higher dust covering factor then as the torus has receded to a farther distance after the outburst, but it may also be reconciled by several alternative modes under the TDE scenario. Guillochon & Ramirez-Ruiz (2015) suggested that there is a delay between the flare and the disruption of the star on the order of years for a BH mass of $10^7\ M_\odot$. If the unbound debris collides with the (torus) ISM, producing shocks and emitting UV and X-rays, it may lead to the enhanced IR emission before the primary outburst. This may also be a potential mechanism to address the early IR brightenings in PS16dtm (Jiang et al. 2017) and PS1-10adi (see Section 3). Other explanations, such as invoking stream collisions as a precursor to the main TDE flare (e.g., Bonnerot & Rossi 2018) or double TDEs induced by stellar binaries incident on SMBH binaries (Coughlin et al. 2018), are also possible. Owing to the deficiency of observational data before the event (e.g., X-rays), a thorough discussion of these possibilities is beyond the scope of this work but could be tested in the future for TDEs with multiwavelength monitoring.

5.2. Infrared Luminosity Compared with Known Supernovas

The SNe scenario was discussed by K17 in parallel with the TDE case. Spectroscopically, PS1-10adi bears a similarity to a type IIn SN (SN IIn; Schlegel 1990; Filippenko 1997), which is distinguished by relatively narrow emission lines and slowly declining light curves. The signatures of SNe IIn are not associated with the explosion itself, but rather with the interaction between ejecta and the dense circumstellar medium (CSM) generally produced by pre-SN mass loss. SNe IIn have gained considerable attention over the past decade partly because they show a huge range in bolometric luminosity (e.g., Li et al. 2011; Richardson et al. 2014), among which the SLSNe are of greatest interest (e.g., Ofek et al. 2007; Smith et al. 2007; Gal-Yam 2012). It is first necessary to demonstrate why PS1-10adi and analogs prefer to be linked to AGNs if they are indeed SLSNe. One possible formation channel of these SLSNe has been proposed to be the runaway mergers of massive stars in dense and young stellar clusters, giving rise to very massive H-rich CSM (Portegies Zwart & van den Heuvel 2007), which seems feasible in high-density central regions of an active galaxy. The dense AGN environment can also provide suitable conditions for high ISM pressure as well as the photoionizing radiation to trap a large fraction of the mass lost from the progenitor (Mackey et al. 2014).

Could the SNe scenario also meet the mid-IR flare freshly revealed by the *WISE* light curve? Fox et al. (2011) have detected 10 out of 68 SNe IIn with late-time (>100 days) IR emission from a warm *Spitzer*/IRAC survey, holding a maximal IR luminosity of $10^8 \sim 10^9\ L_\odot$, that is, around 10^{42} erg s^{-1}. Statistically, the IR emissions of SNe IIn are somewhat more luminous and more sustained than that of other types (e.g., type Ia), due to the heating of preexisting dust by radiative shocks between the expanding SN shell and the dense wind of the progenitor (Fox et al. 2013; Tinyanont et al. 2016). Even so, the peak IR (*W*2 band) luminosity (L_{W2}) of PS1-10adi and analogous objects is uniformly higher than in SNe IIn by at least one order of magnitude, exceeding 10^{43} erg s^{-1}. As a comparison, the L_{W2} maximum of the other AGN transient PS16dtm up to 2017 July (latest public epoch) is also above 10^{43} erg s^{-1} (Jiang et al. 2017) already. We caution that previous *Spitzer* follow-ups (Fox et al. 2011) may have missed the early IR emission, so we subsequently checked the *WISE* light curves of all SNe IIn exploded during 2009 and 2016 from the open supernova catalog [5] (Guillochon et al. 2017). Among them, the most IR-luminous ones (e.g., SN2010jl, SN2013dy, SN2014ab) show no higher luminosity and still possess $L_{W2} \sim 10^{42}$ erg s^{-1} (see Figure 8). As we mentioned in Section 4.2, the controversial event ASASSN-15lh was discovered as a historical SLSNe at first, while more observational facts later favor the TDE scenario. A mid-IR flare after the giant optical outburst has also been detected in ASASSN-15lh by *WISE* with a peak $L_{W2} \sim 10^{43}$ erg s^{-1}, making it stand out from SNe despite being slightly lower than PS1-10adi. In other words, the IR luminosity of PS1-10adi and analogs is significantly higher than that of known certified SNe IIn, as well as any other types of SNe, to our knowledge.

5.3. Dust Covering Factor: Consistent with AGN Torus

The extremely high IR luminosity of PS1-10adi cannot be reconciled with an SNe, but it seems fairly practical for TDEs in AGNs, in which the dusty torus around the BH will unavoidably absorb the TDE emission and reprocess it into the IR. To depict the dust content around PS1-10adi more quantitatively, we try to calculate its dust covering factor

[5] https://sne.space/

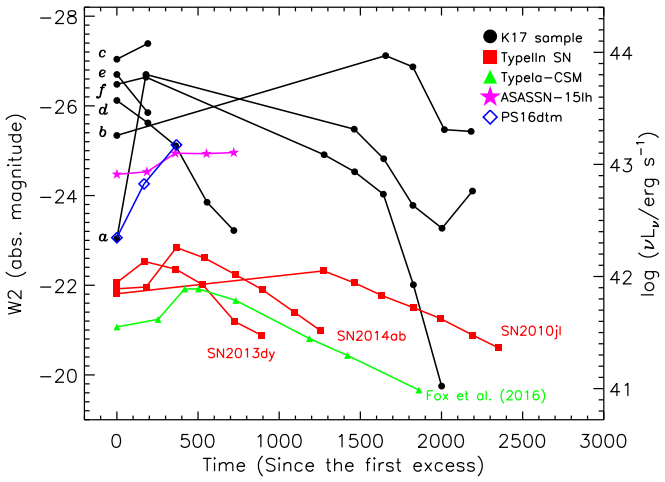

Figure 8. *WISE W2* (4.6 μm) absolute magnitude (background subtracted) of the K17 sample and SNe with prominent mid-IR excesses: (a–f) PS1-10adi, PS1-13jw, CSS100217, J094806, J094608, and J233454, namely the six objects listed in the supplementary Table 1 of K17. The type IIn SNe are plotted as red squares, and type Ia-CSN SNe are shown as green triangles (Fox et al. 2016). We have also overplotted ASASSN-15lh (magenta star) and PS16dtm (blue diamonds) for comparison.

($f_{\rm dust}$), namely the fraction of the sky obscured by dust when seen from the central source. The idea is very straightforward that the original UV-optical photons toward the dust region will be entirely absorbed and reemitted in the IR. Therefore, the ratio between energy radiated through dust reprocessing ($E_{\rm dust}$) and total energy initially released by the event ($E_{\rm rad}$) can be used to indicate $f_{\rm dust}$ (see also van Velzen et al. 2016). K17 has obtained an $E_{\rm rad}$ of $\sim 2.3 \times 10^{52}$ erg by integrating the UV-optical blackbody emission and taking into consideration the early UV excess and missing rise-time contribution. Unfortunately, the precise calculation of $E_{\rm dust}$ is hindered by the sparse sampling and the three-year gap of the mid-IR light curve. As an acceptable alternative, we have calculated the $E_{\rm dust}$ based on the piecewise linear luminosity evolution, yielding a value of 1.0×10^{52} erg. The derived $f_{\rm dust}$ of PS1-10adi is thus $\sim$0.4, which is broadly consistent with AGNs estimated by other methods, such as fitting the torus component to the SEDs of AGNs (e.g., Fritz et al. 2006; Mor et al. 2009; Roseboom et al. 2013). We have subsequently computed the $f_{\rm dust}$ for the other five events in K17 using the same approach and obtained comparable values.

The high $f_{\rm dust}$ of PS1-10adi is a natural consequence of AGNs, which is automatically satisfied in the TDE case as it happens in the accretion disk scale encircled by the torus. Core-collapse SNe are believed to be one of the major production sites of cosmic dust grains (see a recent review by Sarangi et al. 2018), either by ejecting metal-rich materials into space for dust condensation or through the interaction between the ejecta and the dense CSM. However, the amount of dust produced by an individual SNe is very limited and hard to manifest in the SNe as such a high covering factor. The only conceivable SNe likelihood remaining is an SLSNe that exploded inside or exactly in the torus (e.g., Assef et al. 2018). In the meantime, the torus or AGN gas may also provide the dense CSM that is thought to be needed to make the SNe superluminous. The SNe scheme cannot be ruled out completely with the caveat that the SNe explosion within the torus scale has not been well demonstrated.

We do not expect that the mid-IR echoes allow us to definitely diagnose the nature of PS1-10adi and analogs, but they indeed confidently confine the outburst location to be no larger than the torus scale. It is not trivial to differentiate TDEs and SNe with existing information and our current knowledge. Some other studies have even invoked peculiar AGN processes to generate these intense nuclear flares of Seyfert galaxies. For instance, the interaction between BH disk winds and BLR clouds is proposed to reproduce the observed luminosity and timescale (Moriya et al. 2017). In fact, a high-amplitude AGN variability could be misidentified as TDE or vice versa (e.g., Merloni et al. 2015; Saxton et al. 2018). In this way, the ionizing continuum and mid-IR echoes may be the least informative aspect of the transient, and other identifying signatures (e.g., chemical abundance ratio, Yang et al. 2017) are needed.

6. Summary

The investigation of TDEs in AGNs has become more and more realizable thanks to the recent rapid development of time-domain astronomy. Continuing from our first dust echo case study on PS16dtm (Jiang et al. 2017), which is a TDE occurring in a Seyfert 1 host found by Pan-STARRS, we next turned our attention to the other event, PS1-10adi (K17), discovered by the same survey. The outburst of PS1-10adi happens much earlier than that of PS16dtm and thus yields a more complete light curve, which will provide us with an excellent opportunity to understand TDEs in AGNs.

The mid-IR echoes appearing in both events display some distinctive characteristics compared with previous TDEs in quiescent galaxies. The complete understanding of these two events is beyond this work, yet their unusual behaviors can be largely attributed to a preexisting dusty torus in AGNs that is absent in quiescent galaxies. First, the mid-IR flares are detectable even earlier than the optical ones. The dust temperature naively fitted by blackbody emission in the early stage is higher than the dust sublimation temperature, indicating strong ongoing dust evaporation. We infer that it is the torus dust around the BH that has (partially) obscured and weakened the optical emission, which has been conversely transferred to the IR emission. Along with the rising of the TDE bolometric luminosity, the inner radius of the torus receded until the peak luminosity was reached. During this process, the metals originally contained in the dust will be delivered to the gas and give rise to the prominent Fe II multiplets seen in PS16dtm and PS1-10adi. The Fe II lines of PS1-10adi faded until the outburst ended, strongly supporting the photoionizing mechanism, although the collisional excitation may also act, triggered by the interaction between the unbound stellar debris and the torus gas in the TDE scenario.

The other intriguing feature of PS1-10adi is the late-stage UV-optical rebrightening at $\sim$1500 rest-frame days after the primary outburst. The peak luminosity of the hump is $\sim 5 \times 10^{43}$ erg s^{-1}, which is two orders of magnitude lower than the primary peak. In agreement with most other optical TDEs, the X-rays were not detected in the early stage (Auchettl et al. 2017). Interestingly, the *Swift* observation triggered during the rebrightening has captured the X-ray emission. In addition, a mid-IR rebrightening also exists immediately after the the optical one. The late-stage accretion possibility is disfavored by the ultrahigh $T_{\rm dust}$ and X-ray emerging. We have also noticed that at least two other reported TDEs

(ASASSN-15lh and OGLE16aaa) show somewhat similar behavior, yet the rebrightening takes place at a much earlier stage. Unlike the reprocessing or circularization model suggested for ASASSN-15lh, we have proposed a new mechanism responsible for the rebrightening inspired by the fact of the AGN phase before PS1-10adi occurs. In this scenario, the collision between the high-speed outflow and the torus has resulted in the UV-optical rebrightening and X-ray onset. We suspect that it may be a universal phenomenon for the TDEs in AGNs. Further follow-ups of PS16dtm and more events can help us to confirm the idea or not.

The mid-IR light curves analyzed in this work can also help us understand the nature of these highly energetic transient events in the centers of active galaxies. The peak IR luminosities of PS1-10adi and analogs are more than 10 times higher than that of all known IR-luminous SNe, but they could be rare SNe exploded in the torus. Moreover, their IR luminosity is also much higher than that of normal TDEs in quiescent galaxies (e.g., Jiang et al. 2016; van Velzen et al. 2016). It can be easily understood as the dusty torus effect, which solely acts in AGNs. The torus has obscured the central engine of PS1-10adi with a covering factor of $\sim$0.4 and radiatively transferred a large fraction of high-energy photons to the IR band.

A torus is an essential ingredient in the AGN unification model to explain various observational characteristics exhibited in different types of AGNs, although its attributes are still far from clarity. TDEs in AGNs may enable us to probe the torus from a novel perspective. The dust echo of the torus will respond to the tidal disruption radiation as an outstanding mid-IR flare, which is presumably even more remarkable than the optical flare. The time delay of the flare in the mid-IR to the optical is an expression of the torus physical scale, and the total radiated energy in the IR can be used to measure the dust covering factor of AGNs. Similar phenomena have also been reported in other sorts of systems undergoing a dramatic change in accretion rate, namely changing-look AGNs in which the AGN type has transited from type 1 to type 2 or vice versa (Sheng et al. 2017; 2019 in preparation). Moreover, the interaction between the high-speed outflow and ISM may also give useful insights into the torus information. The new approach demands a timely trigger of mid-IR monitoring (e.g., *Spitzer*) of the TDE candidates found in AGNs by the X-ray or optical bands. On the other hand, the mid-IR flares identified from surveys like *WISE* (e.g., Wang et al. 2018; Jiang et al. in preparation) also deserve prompt follow-ups in other bands (e.g., X-rays). The complete coverage of all events at each band is too expensive and unrealistic, yet could be achieved by certain well-defined projects in the upcoming golden era of time-domain astronomy.

We thank the anonymous referee for many constructive comments and suggestions. We thank Dr. Erkki Kankare for providing us the optical spectra data of PS1-10adi. This work is supported by the National Basic Research Program of China (grant 2015CB857005), NSFC (116203021, 11421303, 11733001, 11703022, 11833007), the Joint Research Fund in Astronomy (U1431229, U1731104) under cooperative agreement between the NSFC and the CAS, Anhui Provincial Natural Science Foundation, and the Fundamental Research Funds for the Central Universities. This research makes use of data products from the *Wide-field Infrared Survey Explorer*, which is a joint project of the University of California, Los Angeles, and the Jet Propulsion Laboratory/California Institute of Technology, funded by the National Aeronautics and Space Administration. This research also makes use of data products from *NEOWISE-R*, which is a project of the Jet Propulsion Laboratory/California Institute of Technology, funded by the Planetary Science Division of the National Aeronautics and Space Administration.

ORCID iDs

Ning Jiang https://orcid.org/0000-0002-7152-3621
Tinggui Wang https://orcid.org/0000-0002-1517-6792
Guobin Mou https://orcid.org/0000-0002-0092-7944
Liming Dou https://orcid.org/0000-0002-4757-8622
Zhenfeng Sheng https://orcid.org/0000-0001-6938-8670

References

Assef, R. J., Prieto, J. L., Stern, D., et al. 2018, ApJ, 866, 26
Auchettl, K., Guillochon, J., & Ramirez-Ruiz, E. 2017, ApJ, 838, 149
Baldwin, J. A., Ferland, G. J., Korista, K. T., Hamann, F., & LaCluyzé, A. 2004, ApJ, 615, 610
Blanchard, P. K., Nicholl, M., Berger, E., et al. 2017, ApJ, 843, 106
Bogdán, Á, & Goulding, A. D. 2015, ApJ, 800, 124
Bonnerot, C., & Rossi, E. M. 2018, arXiv:1805.09329
Bonnerot, C., Rossi, E. M., Lodato, G., & Price, D. J. 2016, MNRAS, 455, 2253
Chen, M. C., Broadhurst, T., Lim, J., et al. 2018, ApJ, 863, 135
Collin, S., & Joly, M. 2000, NewAR, 44, 531
Coughlin, E. R., Darbha, S., Kasen, D., & Quataert, E. 2018, ApJL, 863, L24
Dai, L., McKinney, J. C., Roth, N., Ramirez-Ruiz, E., & Miller, M. C. 2018, ApJL, 859, L20
Dong, S., Shappee, B. J., Prieto, J. L., et al. 2016, Sci, 351, 257
Dou, L., Wang, T., Jiang, N., et al. 2016, ApJ, 832, 188
Dou, L., Wang, T., Yan, L., et al. 2017, ApJL, 841, L8
Filippenko, A. V. 1997, ARA&A, 35, 309
Fox, O. D., Chevalier, R. A., Skrutskie, M. F., et al. 2011, ApJ, 741, 7
Fox, O. D., Filippenko, A. V., Skrutskie, M. F., et al. 2013, AJ, 146, 2
Fox, O. D., Johansson, J., Kasliwal, M., et al. 2016, ApJL, 816, L13
Fritz, J., Franceschini, A., & Hatziminaoglou, E. 2006, MNRAS, 366, 767
Gal-Yam, A. 2012, Sci, 337, 927
Godoy-Rivera, D., Stanek, K. Z., Kochanek, C. S., et al. 2017, MNRAS, 466, 1428
Greene, J. E., & Ho, L. C. 2005, ApJ, 630, 122
Greene, J. E., & Ho, L. C. 2007, ApJ, 670, 92
Guhathakurta, P., & Draine, B. T. 1989, ApJ, 345, 230
Guillochon, J., Parrent, J., Kelley, L. Z., & Margutti, R. 2017, ApJ, 835, 64
Guillochon, J., & Ramirez-Ruiz, E. 2015, ApJ, 809, 166
Hayasaki, K., Stone, N., & Loeb, A. 2016, MNRAS, 461, 3760
Heckman, T. M., & Best, P. N. 2014, ARA&A, 52, 589
Hezaveh, Y. D., Marshall, P. J., & Blandford, R. D. 2015, ApJL, 799, L22
Hills, J. G. 1975, Natur, 254, 295
Hönig, S. F., Kishimoto, M., Antonucci, R., et al. 2012, ApJ, 755, 149
Hönig, S. F., Kishimoto, M., Tristram, K. R. W., et al. 2013, ApJ, 771, 87
Jahnke, K., & Macciò, A. V. 2011, ApJ, 734, 92
Jiang, N., Dou, L., Wang, T., et al. 2016, ApJL, 828, L14
Jiang, N., Wang, T., Yan, L., et al. 2017, ApJ, 850, 63
Jiang, N., Zhou, H.-Y., Ho, L. C., et al. 2012, ApJL, 759, L31
Jiang, Y.-F., Guillochon, J., & Loeb, A. 2016, ApJ, 830, 125
Joly, M. 1981, A&A, 102, 321
Kankare, E., Kotak, R., Mattila, S., et al. 2017, NatAs, 1, 865
Kara, E., Dai, L., Reynolds, C. S., & Kallman, T. 2018, MNRAS, 474, 3593
Karas, V., & Šubr, L. 2007, A&A, 470, 11
Komossa, S. 2015, JHEAp, 7, 148
Kormendy, J., & Ho, L. C. 2013, ARA&A, 51, 511
Kruegel, E. 2003, The Physics of Interstellar Dust (Bristol: Institute of Physics)
Krühler, T., Fraser, M., Leloudas, G., et al. 2018, A&A, 610, A14
Leloudas, G., Fraser, M., Stone, N. C., et al. 2016, NatAs, 1, 0002
Li, W., Leaman, J., Chornock, R., et al. 2011, MNRAS, 412, 1441
Lu, W., Kumar, P., & Evans, N. J. 2016, MNRAS, 458, 575
Lyu, J., & Rieke, G. H. 2018, ApJ, 866, 92
Mackey, J., Mohamed, S., Gvaramadze, V. V., et al. 2014, Natur, 512, 282

Mainzer, A., Bauer, J., Cutri, R. M., et al. 2014, ApJ, 792, 30
Mao, S., Witt, H. J., & Koopmans, L. V. E. 2001, MNRAS, 323, 301
Margutti, R., Metzger, B. D., Chornock, R., et al. 2017, ApJ, 836, 25
Mathis, J. S., Rumpl, W., & Nordsieck, K. H. 1977, ApJ, 217, 425
Mattila, S., Pérez-Torres, M., Efstathiou, A., et al. 2018, Sci, 361, 482
Meisner, A. M., Lang, D., & Schlegel, D. J. 2018, AJ, 156, 69
Merloni, A., Dwelly, T., Salvato, M., et al. 2015, MNRAS, 452, 69
Metzger, B. D., & Stone, N. C. 2016, MNRAS, 461, 948
Mor, R., Netzer, H., & Elitzur, M. 2009, ApJ, 705, 298
Moriya, T. J., Tanaka, M., Morokuma, T., & Ohsuga, K. 2017, ApJL, 843, L19
Namekata, D., & Umemura, M. 2016, MNRAS, 460, 980
Netzer, H. 2013, in The Physics and Evolution of Active Galactic Nuclei, ed. H. Netzer (Cambridge: Cambridge Univ. Press)
Netzer, H. 2015, ARA&A, 53, 365
Ofek, E. O., Cameron, P. B., Kasliwal, M. M., et al. 2007, ApJL, 659, L13
Ostriker, J. P. 2000, PhRvL, 84, 5258
Peng, C. Y. 2007, ApJ, 671, 1098
Peterson, B. M. 1997, An Introduction to Active Galactic Nuclei (Cambridge: Cambridge Univ. Press), 238
Phinney, E. S. 1989, in International Astronomical Union Union Astronomique Internationale, The Center of the Galaxy, ed. M Morris (Dordrecht: Springer), 543
Portegies Zwart, S. F., & van den Heuvel, E. P. J. 2007, Natur, 450, 388
Rees, M. J. 1988, Natur, 333, 523
Richardson, D., Jenkins, R. L., III, Wright, J., & Maddox, L. 2014, AJ, 147, 118
Roseboom, I. G., Lawrence, A., Elvis, M., et al. 2013, MNRAS, 429, 1494
Sądowski, A., Tejeda, E., Gafton, E., Rosswog, S., & Abarca, D. 2016, MNRAS, 458, 4250
Sarangi, A., Matsuura, M., & Micelotta, E. R. 2018, SSRv, 214, 63
Saxton, C. J., Perets, H. B., & Baskin, A. 2018, MNRAS, 474, 3307
Schlegel, E. M. 1990, MNRAS, 244, 269
Sheng, Z., Wang, T., Jiang, N., et al. 2017, ApJL, 846, L7
Sigut, T. A. A., & Pradhan, A. K. 2003, ApJS, 145, 15
Smith, N., Li, W., Foley, R. J., et al. 2007, ApJ, 666, 1116
Stern, D., Assef, R. J., Benford, D. J., et al. 2012, ApJ, 753, 30
Stone, N., Sari, R., & Loeb, A. 2013, MNRAS, 435, 1809
Stone, N. C., & Metzger, B. D. 2016, MNRAS, 455, 859
Tejeda, E., Gafton, E., Rosswog, S., & Miller, J. C. 2017, MNRAS, 469, 4483
Tinyanont, S., Kasliwal, M. M., Fox, O. D., et al. 2016, ApJ, 833, 231
van Velzen, S., Farrar, G. R., Gezari, S., et al. 2011, ApJ, 741, 73
van Velzen, S., Mendez, A. J., Krolik, J. H., & Gorjian, V. 2016, ApJ, 829, 19
Véron-Cetty, M.-P., Joly, M., Véron, P., et al. 2006, A&A, 451, 851
Wang, J., & Merritt, D. 2004, ApJ, 600, 149
Wang, T., Yan, L., Dou, L., et al. 2018, MNRAS, 477, 2943
Waxman, E., & Draine, B. T. 2000, ApJ, 537, 796
Wright, E. L., Eisenhardt, P. R. M., Mainzer, A. K., et al. 2010, AJ, 140, 1868
Wyrzykowski, Ł., Zieliński, M., Kostrzewa-Rutkowska, Z., et al. 2017, MNRAS, 465, L114
Yan, L., Donoso, E., Tsai, C.-W., et al. 2013, AJ, 145, 55
Yang, C., Wang, T., Ferland, G. J., et al. 2017, ApJ, 846, 150
Zhao, H., Haehnelt, M. G., & Rees, M. J. 2002, NewA, 7, 385
Zhou, H., Wang, T., Wang, H., et al. 2006, ApJ, 639, 716